Adaptation of Cardiac Structure by Mechanical Feedback in the Environment of the Cell: A Model Study

Theo Arts, Frits W. Prinzen,* Luc H. E. H. Snoeckx,* Jons M. Rijcken, and Robert S. Reneman*
From the Departments of Biophysics and *Physiology, Cardiovascular Research Institute Maastricht (CARIM), University of Limburg, The Netherlands

ABSTRACT In the cardiac left ventricle during systole mechanical load of the myocardial fibers is distributed uniformly. A mechanism is proposed by which control of mechanical load is distributed over many individual control units acting in the environment of the cell. The mechanics of the equatorial region of the left ventricle was modeled by a thick-walled cylinder composed of 6–1500 shells of myocardial fiber material. In each shell a separate control unit was simulated. The direction of the cells was varied so that systolic fiber shortening approached a given optimum of 15%. End-diastolic sarcomere length was maintained at 2.1 μm. Regional early-systolic stretch and global contractility stimulated growth of cellular mass. If systolic shortening was more than normal the passive extracellular matrix stretched. The design of the load-controlling mechanism was derived from biological experiments showing that cellular processes are sensitive to mechanical deformation. After simulating a few hundred adaptation cycles, the macroscopic anatomical arrangement of helical pathways of the myocardial fibers formed automatically. If pump load of the ventricle was changed, wall thickness and cavity volume adapted physiologically. We propose that the cardiac anatomy may be defined and maintained by a multitude of control units for mechanical load, each acting in the cellular environment. Interestingly, feedback through fiber stress is not a compelling condition for such control.

INTRODUCTION

Fiber stress and shortening are likely to be similar everywhere within the wall of the normal heart (Arts and Reneman, 1989; Van der Vusse et al., 1990). After an increase of hemodynamic load, the left ventricular pump adapts to the new situation. Heart rate, contractility, and preload may change acutely. If the increase in load lasts longer, on the order of days, weeks, or months, chronic adaptation can be observed. The mass of the myocardium increases, whereas the acute adaptation effects partly disappear. An increase in aortic pressure causes an increase in wall mass, whereas cavity volume remains practically the same (concentric hypertrophy) (Sasayama et al., 1976; Gelpi et al., 1991; Aoyagi et al., 1992). If aortic volume flow is required to increase while systolic aortic pressure is constant, both wall mass and cavity volume will increase (eccentric hypertrophy). The adaptations to changes in hemodynamic load are reversible (Shigematsu et al., 1990). Cardiac mass generally returns to normal after surgical repair of cardiac valve defects (Gaasch et al., 1978; Monrad et al., 1988). During these changes in cardiac mass, the complicated helical organization of the muscle fibers (Torrent-Guasp, 1959; Streeter, 1979) is maintained. An obvious mechanism to control the global cardiac structure is the permanent comparison of the current structure with the structure as defined by a reference design. The global structure will be adapted if deviations from a stored reference are detected. However, such a hypothesis is not attractive, because no biological mechanism is known that senses the global structure of the heart and selectively changes parts of the structure.

We investigated whether control of mass and shape of the heart as an entity could be obtained by the summed action of many individual regional controlling units for fiber stretch and shortening. The presence of controlling units acting in the direct environment of each cardiac cell is biologically much more attractive. Regionally the cell may sense several physical parameters that are compared with reference values stored within the cell. The controlling actions are directed to the environment of the cell. Then the summation of the controlling actions of the numerous cardiac cells should guarantee preservation of the macroscopic anatomical structure. An attractive aspect of this hypothesis is that the cell is likely to have the tools for such individual cellular controlling actions. Cells can respond to various physical stimuli, related to mechanics, for instance. Cells have messengers that control the growth and formation of various intra- and extracellular structures. The messenger distribution is controlled by the DNA-RNA machinery.

Stretch is likely to be involved in control of cellular growth (Watson, 1991; Yazaki et al., 1993). Stretching of cardiac myocytes causes immediate expression of the proto-oncogene c-*fos*, the amount of which depends on the degree and duration of stretching (Komuro et al., 1990). Besides, other transcription factors, like c-*jun* and c-*myc*, are also induced rapidly (Sadoshima et al., 1992a). The expression of proto-oncogenes may induce cell growth as indicated by the finding that stretch enhances nuclear RNA labeling and translation of genes, such as skeletal α-actin, atrial natriuretic factor, and β-myosin heavy chain (Mann et al., 1989; Sadoshima et al., 1992a). Stretch induces ion transport through the cell membrane (Sigurdson et al., 1992), but the role of

Received for publication 8 September 1993 and in final form 27 January 1994.

Address reprint requests to Theo Arts, Department of Biophysics, Cardiovascular Research Institute Maastricht, University of Limburg, 6200 MD Maastricht, Theo Netherlands.

0006-3495/94/04/953/09 $2.00

this pathway in growth is subject to discussion (Sadoshima et al., 1992b). Contractile activity also accelerates growth of cardiac myocytes (McDermott et al., 1989), indicating that besides stretch, fiber shortening (strain) and/or contractility may also regulate cardiac growth. In the early phase of adaptation to pressure overload collagen (Weber et al., 1988; Chapman et al., 1990; Mukherjee and Sen, 1990; Contard et al., 1991) and fibronectin (Contard et al., 1991; Samuel et al., 1991) are expressed.

Many indications can be found for the presence of control mechanisms acting in the cellular environment, in which mechanical load is involved. For instance, sarcomere length being defined as the repetition length of the cross-striations of cardiac muscle is controlled to approximately 1.95 μm in the unstressed left ventricle (Yoran et al., 1973; Grimm et al., 1980). The regional character of adaptation of the cardiac tissue mass to mechanical load is also indicated during asynchronous electrical activation of the ventricle caused by pacing or conduction blockade of the left bundle branch. Regional differences in mechanical load and coronary perfusion then are found (Prinzen et al., 1990). Tissue mass decreases in the regions with relatively low load (Prinzen et al. In press).

Fiber direction was shown to be an important determinant of the distribution of fiber stress and shortening in the wall of the left ventricle (Arts and Reneman, 1989; Huyghe et al., 1991; Bovendeerd et al., 1992). After a change in hemodynamic load cardiac shape changes, whereas the transmural course of fiber direction seems to be maintained. The mechanism controlling cardiac myocyte alignment is not known yet, but mechanical load is likely to be involved. The response of a cell to a mechanical force can depend on the direction of the force (Rubany et al., 1990). At the inner surface of an artery endothelial cells align with shear force due to flow (Flaherty et al., 1972).

In the present study it will be investigated whether in a simulation a controlling mechanism can be found for the individual cardiac cell, which results in maintenance of the global cardiac structure and proper adaptation to chronic changes in hemodynamic load. Because the main function of the myocardium is mechanical, feedback is postulated to be mechanical too. Most of the feedback signals considered are related to strain. Stretch is quantified by the maximum value of sarcomere length as occurring during the cardiac cycle. Systolic shortening is quantified as the decrease in sarcomere length during the ejection phase. Global myocardial deformation is quantified by the average value of sarcomere shortening. Contractility is considered to be a global stimulus to the heart, and is expressed as the factor by which the reference value of fiber stress has to be multiplied to obtain the required left ventricular systolic pressure. Left ventricular mechanics is simulated in a cylindrical wall consisting of 6–1500 cylindrical shells of myocardial tissue, each of which simulates a cell with its own regional control mechanism. Regional adaptation stimuli are determined per shell by comparing the calculated mechanical parameter values with internal reference values, which are assumed to be common to all cells. Changes in hemodynamic load should induce responses to control mechanical load in the environment of the cell, causing an adaptive change in the shape of the wall, although preserving the cardiac fiber structure. Stability of control is assessed by disturbing the transmural course of fiber direction in the wall, although also changing hemodynamic load stepwise. Finally, the calculated structure is compared with anatomical findings.

DESIGN OF THE MODEL OF LEFT VENTRICULAR MECHANICS

Geometry

The basics of the model of left ventricular mechanics have been described in detail before (Arts et al., 1979; Arts and Reneman, 1989). Briefly, the left ventricle is represented by a thick-walled cylinder with cavity volume V_{lv} and wall volume V_w. The thick-walled cylinder is the simplest geometry in which left ventricular kinematics can be described including the essential torsion and base to apex elongation. Because of similarity of geometry the equatorial region of the ventricle is simulated most accurately (Fig. 1). The myocardial material is represented by contractile fibers embedded in compliant incompressible material. For simplicity passive mechanical properties of the myocardium are ignored in describing the mechanics of ejection. The variables in the cylindrical wall are described as a function of the depth parameter v attached to the wall material. The value of v varies linearly with the enclosed wall volume V from −0.5 at the endocardium to +0.5 at the epicardium:

$$v = V/V_w - 0.5 \quad (1)$$

where V_w is total wall volume.

Kinematics of the wall

The kinematics of the wall follows a pattern (Fig. 2) as partly described earlier (Arts et al., 1992). Deformation is referred to a reference state (ref), for instance the end of diastole. In a layer at depth v the symbol $\beta_{ref}(v)$ indicates the angle between fiber direction and circumference. For the projection of sarcomere length l_{fref} on the axial z- and circumferential c-direction it holds, respectively:

$$l_{zref} = l_{fref}\sin(\beta_{ref}) \quad l_{cref} = l_{fref}\cos(\beta_{ref}) \quad (2)$$

Four modes of deformation are considered (Fig. 2). In the ejection mode

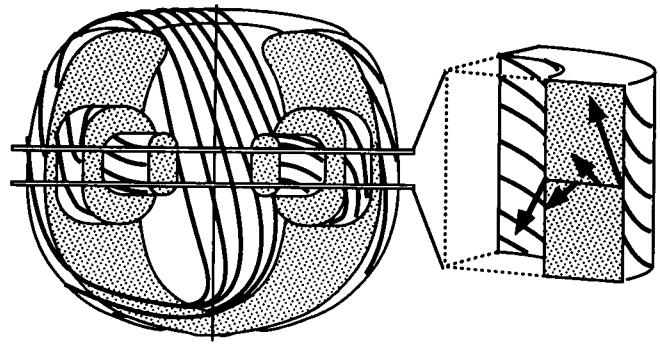

FIGURE 1 Schematic representation of the fiber structure of the left ventricle, and how this structure is implemented in the cylinder. The fibers in the outer layers continue in the inner layers crossing the wall near base and apex. The equatorial section approaches cylinder symmetry as applied in the presented model.

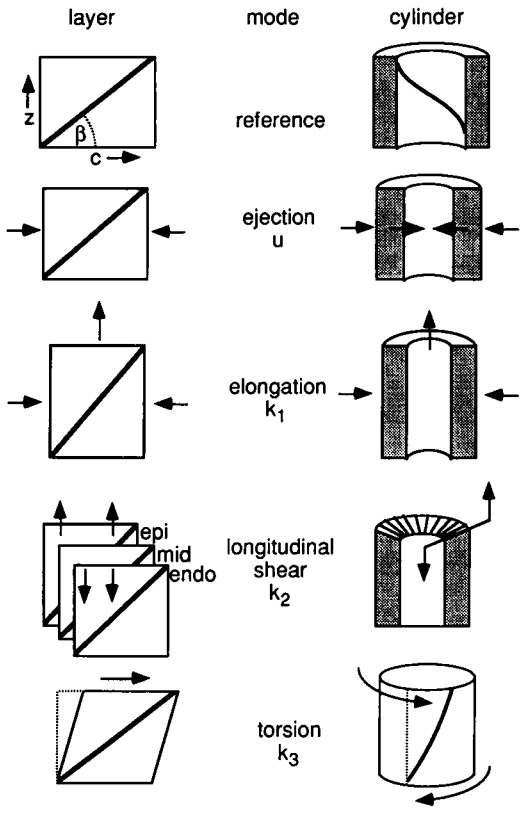

FIGURE 2 Kinematics of the cylinder simulation of the contraction of the left ventricle. The left panel shows planar deformation of a layer in the wall. The right panel shows the related macroscopic deformation of the cylinder. The angle β indicates fiber angle; z and c indicate axial and circumferential coordinates.

cavity volume (V_{lv}) decreases without a change in axial length. The amplitude of this mode is quantified by the dimensionless variable u:

$$u = V_{lv}V_w + 0.5 \tag{3}$$

In the elongation mode the ventricle lengthens by a factor $1 + k_1$ without a change in cavity volume. Because myocardial fibers are wrapped toroidally around the central layers of the wall in the real left ventricle (Fig. 1) (Torrent-Guasp, 1959; Chadwick, 1982; Peskin, 1989), in the axial shear mode (k_2) the inner layers may shorten axially, whereas the outer layers lengthen, and the central layer ($v = 0$) does not deform (Waldman et al., 1985) (see the Appendix). Finally the mode with torsion k_3 causes shear in the plane of the wall. Applying the deformation modes in the sequence mentioned, for the axial and circumferential components of sarcomere length it holds:

$$\begin{aligned} l_z &= l_{ref}\sin(\beta_{ref})\left(\frac{1+k_1}{1+4k_2(v/u)}\right) \\ l_c &= l_{ref}\cos(\beta_{ref})\left(\frac{(u+v)(1+2k_2v^2)}{(u_{ref}+v)(1+k_1)(u^2+uv)}\right)^{0.2} + k_3 l_z \end{aligned} \tag{4}$$

Defining fiber extension e_f as the ratio of sarcomere length to the reference value, it is found for e_f and the fiber angle β:

$$e_f = ((l_z/l_{fref})^2 + (l_c/l_{fref})^2)^{0.5} \quad \beta = \arctan(l_z/l_c) \tag{5}$$

Equations 4 and 5 describe fiber extension as a function of the kinematic parameters u, k_1, k_2, k_3, and the fiber angle $\beta_{ref}(v)$, where the parameter v expresses the transmural position in the wall. The more common fiber strain ϵ_f is related to fiber extension by $\epsilon_f = e_f - 1$.

Equilibria of forces

In each state of deformation during the cardiac cycle the modes related to the parameters k_1–k_3 are associated with force equilibria, providing the solution for the latter parameters. Close to the state of equilibrium the increment in deformation energy ΔE of the wall depends on fiber stress σ_f and the increment of fiber extension Δe_f:

$$\Delta E = \int_{wall} \sigma_f \Delta e_f \, dV$$

with

$$\Delta e_f = l_f/l_{feq} - 1, \quad \Delta e_f \ll 1 \tag{6}$$

where l_f and l_{feq} refer to sarcomere length in the current state and in the yet unknown state of equilibrium, respectively. Equilibrium is reached if total deformation energy is minimum. Then for the kinematic parameter k it is found:

$$\frac{\partial E}{\partial k} = V_w \int_{-0.5}^{+0.5} \sigma_f \frac{\partial e_f}{\partial k} \, dv = 0 \tag{7}$$

Considering for this derivation the state of equilibrium as the reference with $k = 0$, three conditions for equilibrium are derived from Eqs. 4 and 5 applied to Eq. 7:

$$\begin{aligned} \frac{\partial E}{\partial k_1} = 0 &\Rightarrow \int_{-0.5}^{+0.5} \sigma_f(2\sin^2\beta - \cos^2\beta)\, dv = 0 \\ \frac{\partial E}{\partial k_2} = 0 &\Rightarrow \int_{-0.5}^{+0.5} \frac{\sigma_f}{u}\left(4v\sin^2\beta - \frac{v^2}{u+v}\cos^2\beta\right) dv = 0 \\ \frac{\partial E}{\partial k_3} = 0 &\Rightarrow \int_{-0.5}^{+0.5} \sigma_f \sin\beta\cos\beta \, dv = 0 \end{aligned} \tag{8}$$

The Eqs. 8 are used to solve k_1, k_2, and k_3 numerically.

Left ventricular pressure

Conservation of energy can also be used to calculate left ventricular pressure. Analogous to Eq. 7, for the derivative of energy with respect to left ventricular volume it holds:

$$\frac{\partial E}{\partial V_{lv}} = V_w \int_{-0.5}^{+0.5} \sigma_f \frac{\partial e_f}{\partial V_{lv}} \, dv = P_{lv} \tag{9}$$

Applying Eq. 3 to relate V_{lv} to parameter u, Eq. 4 and 5 were used to convert Eq. 9 into:

$$P_{lv} = \frac{1}{2}\int_{-0.5}^{+0.5} \sigma_f \frac{\cos^2\beta}{u+v} \, dv \tag{10}$$

Adaptation in the cellular environment

The cardiac contraction started in end-diastole by setting of the initial values for cavity volume (V_{lved}) and for fiber direction (β_{ed}) as a function of the position parameter v. Sarcomere length l_f was set to the reference length (2.1 μm). During isometric contraction the stress σ_f developed by the fibers in the myocardial tissue depends on sarcomere length (Pollack and Krueger, 1976; Ter Keurs et al., 1980; De Tombe and Ter Keurs, 1991). During active shortening (auxotonic contraction) fiber stress is reduced (Hill, 1950). In the model applied, fiber stress was approximated to be equal to half of the isometrically developed stress:

$$\sigma_f = C_f(l_f/2.1\ \mu m - 0.8) \times 0.25\ 10^6\ Pa \tag{11}$$

where the factor C_f expresses contractility. Initially C_f was set to unity. The

deformation parameters k_1, k_2, and k_3 were solved numerically using Eq. 8. Left ventricular pressure P_{lv} was calculated using Eq. 10. At the beginning of ejection (be) generated left ventricular pressure (P_{lv}) was matched with the required level (P_{lvref}) by adaptation of contractility:

$$C_{fnew} = C_f P_{lvref}/P_{lv}) \tag{12}$$

The beginning of the ejection phase was used as the reference state for deformation during the ejection phase. At the end of ejection (ee), left ventricular volume was decreased by the prescribed stroke volume V_{str}, and again Eq. 8 was solved numerically. Deformation parameters (k_1–k_3), contractility C_f, fiber direction β_{ed}, and sarcomere shortening (l_{sbe}-l_{see}) were stored for further analysis.

Optimization requires a quantity expressing mismatch to be minimized by variation of at least one parameter. It was investigated whether in the cellular environment such a quantity could be defined expressing chronic mismatch between mechanical load and the generator of mechanical work in the myocyte. A set of regional parameters should be found that may be varied to minimize this mismatch. The regional effects of adaptation may be interpreted as a structural rearrangement and growth. The main question to be solved is whether effectuation of all regional optimization units would result in stable control of the macroscopic structure. We propose the following control loop for optimal match of mechanical load (Fig. 3).

For simplicity, the wall is subdivided into a discrete number of shells, each having the same volume V_{sh}. Mismatch (Err) was represented by the sum of the squared normalized deviations of fiber shortening from a given reference (Δl_{ref}), of sarcomere length at the beginning of ejection (l_{sbe}) from a given reference (l_{sberef}), and of the regional fiber direction (β) from the average of both adjacent shells (β_{inner}, β_{outer}):

$$\mathrm{Err} = \ln^2\left(\frac{l_{sbe} - l_{see}}{\Delta l_{ref}}\right) + \ln^2\left(\frac{l_{sbe}}{l_{sberef}}\right) + \left(\beta - \frac{\beta_{inner} + \beta_{outer}}{2}\right)^2 \tag{13}$$

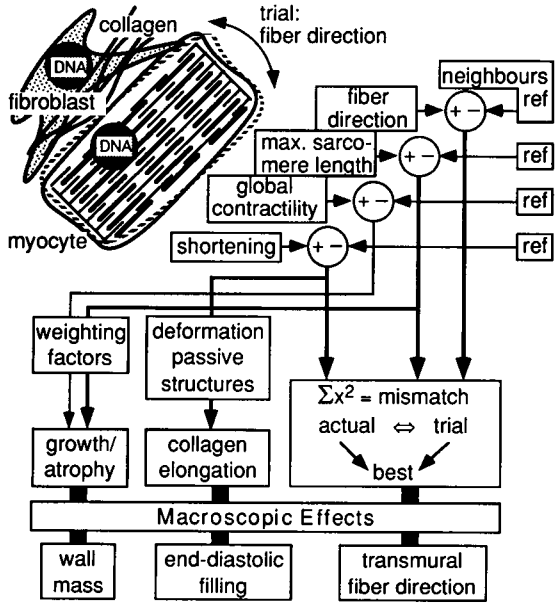

FIGURE 3 Schematic representation of the proposed regional controlling mechanism of reorientation and growth of the cardiac cell. Maximum sarcomere length and fiber shortening are optimized by trials of cellular reorientation. Diastolic dilation of the cavity is related to collagen elongation to be induced by excess of deformation of the wall over a given threshold. Cellular growth may be induced by a weighted combination of global contractility and early-systolic stretch, which is quantified by maximum sarcomere length. Fiber shortening and fiber stress were found not to be needed for control of growth. At the bottom of the figure macroscopic effects are related to the microscopic changes per cell.

The use of squared logarithms in Eq. 13 is a means to normalize deviations from a reference. The angle β doesn't need such normalization because it is already dimensionless. The last term punishes a deviation of the fiber direction from that in the adjacent shells. To reduce Err regionally, trials of fiber direction β_{ed} were induced randomly with an angular dispersion of $\pm 0.5\ C_\beta$ around the current values:

$$\beta_{trial} = \beta_{ed} + C_\beta \cdot \mathrm{Random} \tag{14}$$

with $|\mathrm{Random}| < 0.5$. The trials were subjected to the already determined deformation as expressed by the parameters u, and k_1 through k_3. If somewhere a trial resulted in a lower regional value of Err (Eq. 13), the trial was preferred. Regional growth may be controlled by a weighted sum (G) of the deviations of contractility, fiber shortening, and early-systolic sarcomere length from their reference values:

$$G = w_c \ln(C_f) + w_s \ln[(l_{sbe} - l_{see})/\Delta l_{ref}] + w_b \ln(l_{sbe}/l_{beref}) \tag{15}$$

The term with w_b is related to stretch during the isovolumic contraction phase referred to as early-systolic stretch. In the present study the choice of the values for the weighting factors w_c, w_s, and w_b was a subject of investigation. The comparison of G with a random number was used as a criterion to change mass. Growth or decline of muscle mass was simulated by duplication or skipping of the considered shell, respectively:

$$\text{if } G \begin{cases} > +\mathrm{Random}: \text{growth} \\ \text{in between}: \text{no change} \\ < -\mathrm{Random}: \text{decline} \end{cases} \quad \text{with } 0 < \mathrm{Random} < 1 \tag{16}$$

End-diastolic filling volume was controlled by the amount of deformation during the ejection phase. If deformation was above normal, the tissue dilated passively along the direction of maximum deformation. This rule was expressed by an increase ΔV_{lved} of end-diastolic left ventricular volume when average sarcomere shortening exceeded the normal value:

$$\Delta V_{lved} = C_d V_w \overline{\ln[(l_{sed} - l_{see})/\Delta l_{ref}]} \tag{17}$$

The constant C_d determines the rate of feedback. After adaptation of end-diastolic left ventricular cavity volume, the number of shells, and the transmural course of fiber direction, new adaptation cycles were simulated repeatedly.

METHODS

In the model, the wall of the left ventricle was composed of a finite number N_{sh} of adjoining shells, each having a fixed volume V_{sh}. The integrals (Eqs. 8 and 10) were replaced by a summation over the shells. Applied parameter values are recorded in Table 1. The model was programmed (Fig. 4) in the (ANSI) C-language (THINK C 5.0.2, Symantec) on an Apple Macintosh computer (Powerbook 170).

Initially, using only 6 shells, the fiber angles in the inner half and outer half of the cylinder were set to +0.7 and −0.7 rad, respectively. Cavity volume, sarcomere length, and contractility were set to the reference values. In the early systolic phase, left ventricular pressure, deformation, fiber stress, and sarcomere length were calculated. Contractility was adjusted so that left ventricular pressure reached the systolic reference value. Then, the ventricle was allowed to eject by removing stroke volume from left ventricular cavity volume, and the calculations were repeated for the state of end of ejection. After calculation of fiber mechanics in the separate shells, fiber direction and end-diastolic filling volume were adjusted. The mass of the wall was adapted by insertion or skipping of shells. Calculation of the new state at the beginning of ejection initiated a new adaptation cycle.

After approximately 400 adaptation cycles, a stationary solution was approached with 27–29 shells (Table 1). Then the volume of a shell (V_{sh}) was reduced to 0.5 ml. After 400 adaptation cycles a stationary situation was reached with approximately the same wall and cavity volume but with many more thinner shells (545–550). This state was used as control.

Fluctuations of the transmural course of fiber direction, fiber stress, fiber shortening, and the signals controlling fiber direction (Err in Eq. 13) and growth (G in Eq. 15) around the stationary state were calculated for 10 plots

TABLE 1 Parameter values as used for the simulation of cardiac growth control

Symbol	Value	Meaning
Hemodynamics and muscle mechanics		
V_{str}	100 ml	Stroke volume
P_{lvref}	17.5 kPa	Cavity pressure reference
l_{sed}	2.10 μm	End-diastolic sarcomere length
Δl_{ref}	0.315 μm	Sarcomere shortening
σ_f	See Eq. 14	Stress-sarcomere length relation
Feedback rate constants		
C_β	0.1 rad	Dispersion angle fiber direction trials
C_d	0.5 rad	Passive ventricular dilation
w_b	1.0 rad	Growth/decline with stretch at be
w_c	0.1 rad	Growth/decline with contractiliy C_f
w_s	0.0 rad	Growth/decline with shortening
Geometry		
V_{sh}	10/0.5 ml	Volume of a shell in the wall
V_{lved}*	145 ml	End-diastolic left ventricular volume
N_{sh}*	28/547	Number of shells in the wall ($V_w = N_{sh}V_{sh}$)
Kinematics		
k_{1ee}*	−0.127	Axial strain, end ejection
k_{2ee}*	−0.003	Transmural gradient axial strain, end ejection
k_{3ee}*	+0.121	Torsion at end of ejection.

* Calculated approximately stationary situation.

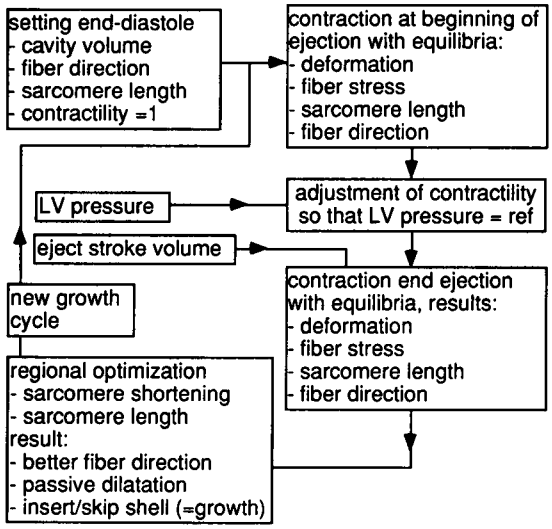

FIGURE 4 Schematic representation of the calculation set-up used in the simulation of cardiac growth and adjustment to hemodynamic load.

of these parameters. The plots were separated by intervals of 40 adaptation cycles. In investigating whether fiber direction changed with left ventricular pressure, a stationary solution for the transmural course of fiber orientation was also calculated for a ventricular pressure of 25 kPa.

The transmural course of fiber direction as calculated was compared with experimental data reported in literature. To enable such comparison, the volume scale from endo- to epicardium was modified to a scale proportional to the radius in the wall.

Adaptation of the volume of wall and cavity to changes in hemodynamic load was assessed by recording these parameters and left ventricular pressure at normal contractility, while forcing changes in stroke volume or systolic left ventricular pressure. Starting with 50 adaptation cycles with normal load, left ventricular pressure was increased suddenly from 17.5 to 25 kPa (1 kPa = 7.5 mm Hg) for 50 cycles, and was returned stepwise to control for the next 50 cycles. Similarly, stroke volume was suddenly increased from 100 to 200 ml for 50 cycles, and stepwise returned to control for another 50 cycles.

Finally, the stability of the feedback loop was investigated for various values of the feedback parameters. Starting from the values as presented in Table 1, variations were applied to the dispersion angle of the fibers, feedback of diastolic dilation, and growth feedback of early systolic fiber stretch, sarcomere shortening, and contractility. To save computing time, the simulations were carried out starting with only 14 shells in the wall, being the stationary solution with a shell volume V_{sh} of 20 ml. The investigated parameters were changed simultaneously with a twofold increase of stroke volume to 200 ml. If within 100 adaptation cycles the solution approached the earlier found stationary one, the solution was considered stable.

In an extreme test for stability of control, it was investigated whether a falsely directed layer in the myocardium could be corrected. For that purpose, adaptation cycles were initiated with the following transmural distribution of the fiber angles over 14 shells from the endocardium to the epicardium: +1.0, −1.0, −1.0, +1.0, +1.0, +1.0, +1.0, +1.0, −1.0, −1.0, −1.0, −1.0, +1.0, and −1.0 rad. If after 100 adaptation cycles the aberrant fiber directions in the outer and inner layers disappeared, the correction was judged to work.

RESULTS

Starting with 6 shells, and a fiber direction of +0.7 rad and −0.7 rad in the inner and outer layers, respectively, the transmural course of fiber direction developed within 50 adaptation cycles to a distribution close to the one reached in the stationary state after 400 cycles. Then the shell volume was decreased to 0.5 ml. The state reached after 400 cycles was used as the starting reference state for this study (Table 1). In Fig. 5 ten transmural courses of fiber direction, sarcomere shortening, developed fiber stress, and the signals controlling fiber direction (Err in Eq. 13) and growth (G in Eq. 15) are depicted at intervals of 40 cycles. Although an approximately stationary solution was found, a single unique solution was never reached. The standard deviations of the noise in the

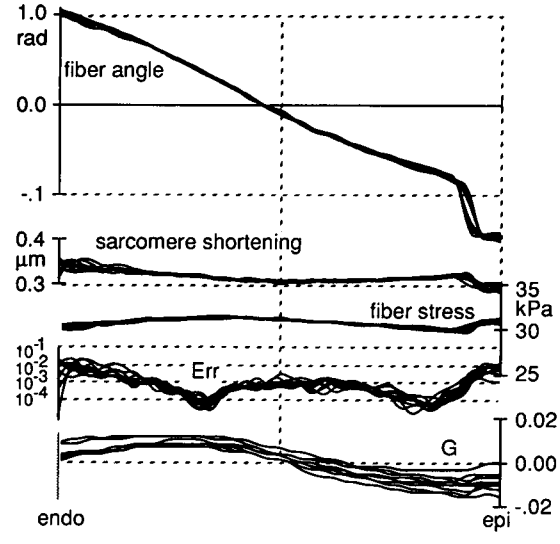

FIGURE 5 Stationary solution of the transmural courses of fiber angle, sarcomere shortening, systolic fiber stress, and the control signals,regional mismatch Err and growth stimulus G. The transmural coordinate is proportional to the enclosed wall volume. Ten curves are shown, each separated by 40 adaptation cycles. Strikingly, the average seems to be quite stable, but small fluctuations are always found around this average.

fiber direction, sarcomere shortening, and fiber stress were ± 0.020 rad, ±0.0035 μm, and ± 501 Pa, respectively. The fiber direction varied on the average from 1.02 rad at the endocardium to −1.48 rad at the epicardium (1 rad = 57.3°). Close to the site where half of the volume of the wall was enclosed, the fibers were directed circumferentially. Just below the outer surface a steep gradient in fiber angle was visible. Average sarcomere shortening was almost equal to the reference value (0.316 vs. 0.315 μm), with a systematic pattern of transmural variations as small as ±0.012 μm SD. This moderate nonuniformity was also reflected in the transmural course of fiber stress. The transmural course of regional mismatch Err (Eq. 13) was plotted on a logarithmic scale. Err was maximum in the far inner and outer layers, and minimum at a depth of 0.3 and 0.8 in the wall as counted from the inner surface. The signal for growth feedback G (Eq. 15) was on the average slightly positive in the inner layers and negative in the outer ones.

In Fig. 6 systolic left ventricular pressure, wall volume end-diastolic cavity volume, contractility (Eq. 12), and the feedback signals are shown as a function of the number of elapsed adaptation cycles, which is assumed to be related to time. Even if load was constant, the variables varied slightly around an average value. When increasing pressure load, wall volume increased similarly. Cavity volume decreased. The latter changes reflect concentric hypertrophy resulting from hypertension, for example. After return to control, the changes were reversed. A sudden increase in stroke volume was followed by a temporary increase in contractility and a chronic ventricular dilation. Both cavity and wall volume remained elevated, reflecting eccentric hypertrophy. After a sudden return to control, contractility decreased, but after some oscillations all variables returned to normal. The mismatch signal Err increased after a sudden change in volume load, indicating deviation from a nearly optimal setting. During pressure load the Err signal was elevated chronically. The dilation signal was active during changes in volume load rather than in pressure load.

In Fig. 7, the transmural course of fiber direction is plotted as a function of the radius in the wall, as found in various animals under different conditions, and as calculated in the present study. All curves started at an angle in the range from +0.5 to +1.5 rad at the endocardium, reaching 0 rad at midwall, ending in an angular range from −0.8 to −1.5 rad at the epicardium (1 rad = 57.3°). In a simulation with normal left ventricular pressure (17.5 kPa, 1 kPa = 7.5 mm Hg) in the outer half the transmural course of the fiber angle was similar to the experimental data, the bending of the curve inclusive. In the inner half there was some difference. When elevating systolic pressure to 25 kPa, the solution was approximately the same, except for the extreme inner and outer layer.

Starting from the feedback parameter settings in Table 1, each time only one parameter was changed, while keeping all others at the standard setting. The passive dilation feedback constant should be in the range of $0.01 \leq C_d < 4.0$. The dispersion angle of the fibers should be in the range of $0 < C_\beta \leq 1.0$ rad. For $C_\beta < 0.1$ rad, the speed of control of fiber direction was inversely proportional to C_β. Similarly, the parameter controlling growth by contractility should be in the range of $0.01 < w_c \leq 1.0$. For larger values control was unstable, and for the smaller values control of growth was too slow or absent. The parameter controlling growth by early systolic stretch should be in the range of $0.1 < w_b < 8.0$. In correcting for severe disorientation of the fibers in a few distinct layers, the ranges for proper corrections were found to be narrower. Best control was obtained around the standard setting. Remarkably the early systolic stretch feedback constant had a distinct narrow range of $0.8 < w_b < 1.2$. Outside this range the disoriented layers were maintained. Because feedback of systolic shortening did not have any beneficial effect to the control of myocardial mass, $w_s = 0$ was used.

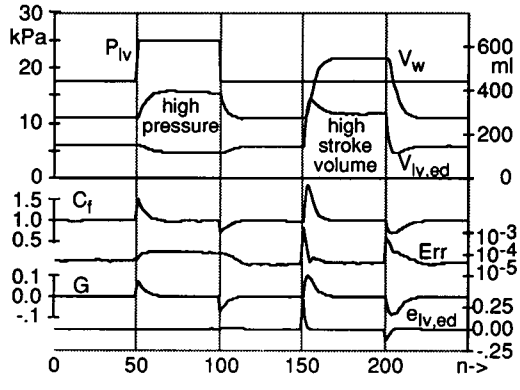

FIGURE 6 Left ventricular pressure (P_{lv}), wall volume (V_w), end-diastolic cavity volume ($V_{lv,ed}$), contractility (C_f), and the transmural averages of control signals regional mismatch (Err), growth stimulus (G), and end-diastolic cavity volume dilation ($e_{lv,ed}$) are shown as a function of the number of adaptation cycles elapsed in the simulation. Periods of high pressure and high stroke volume load are indicated. During pressure load hypertrophy is eccentric, during volume load concentric. During periods of constant load, slight fluctuations around an average are visible.

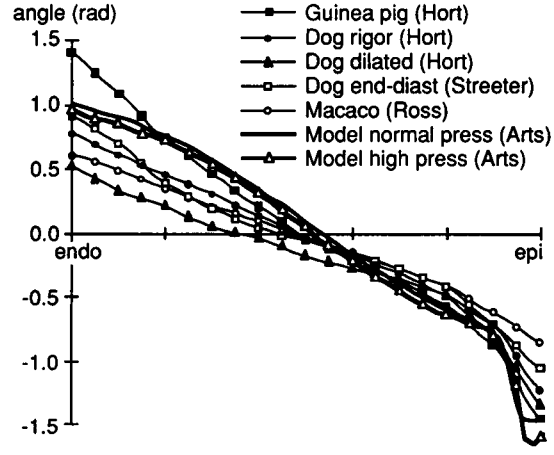

FIGURE 7 Comparison of experimental data with simulated results on the transmural course of fiber direction. Different symbols refer to different species and circumstances as indicated in upper right corner. Normal and high pressure refer to 17.5 and 25 kPa systolic pressure in the simulation as presented in this article.

DISCUSSION

In a numerical simulation it was shown that during changes in pressure and volume load a macroscopic anatomical structure of a cylindrical left ventricle could be maintained by feedback of mechanical signals acting at a short range around the cell. Given that the hemodynamic load is determined by systolic pressure and stroke volume, the fiber structure in the cylindrical wall is determined by set points of end-diastolic sarcomere length, sarcomere shortening, and contractility. The rate of feedback was controlled by four parameters (Table 1). To guarantee proper control the feedback constants could be in a wide range. Despite this wide range of operation, stability of control of shape and fiber structure was best with a parameter setting in a much narrower range near the setting as shown in Table 1.

In the real left ventricle, the following three parameters may vary quite independently. Diastolic filling volume is likely to be controlled mainly by lengthening of the collagen fibers in the tissue with increasing deformation along the fibers. Wall mass should enable generation of the work needed. Sarcomere length should be in the physiological range. Therefore, the controlling system needs at least three set points. This study presents such a system. However, it is very possible that other controlling structures are also satisfactory, as long as three or more set points are incorporated.

The main result of this study is that a complicated anatomical structure can be coded by the settings and structure of a controlling system operating in the vicinity of each cell. In each region cells respond similarly to mechanical signals, but the result is an organized structure in which each part seems to have a distinct function. It should be noted that the model used is cylinder symmetric. So it is not proven that such a system works for the complicated three-dimensional cardiac structure. The proposed controlling system is attractive because several of its characteristics (Fig. 3) were found to exist. Both stretch and contractility are likely to play an important role in the control of myocardial growth. This is consistent with molecular biological findings, indicating that stretch and contraction of cardiomyocytes are clearly involved in mechanical signaling and protein synthesis (see the introduction). Control of myocardial sarcomere length is indicated by its narrow range around 1.95 μm at zero filling pressure in diastole (Yoran et al., 1973; Grimm et al., 1980). The possibility of using trials as a tool to optimize fiber direction is indicated by the presence of a dispersion by a few degrees. Furthermore the cardiac myocytes are relatively short ($\approx$120 μm) (Campbell et al., 1991), enabling redirection of the cell with respect to the environment. Such optimization of cellular orientation can also be understood as slowing down continuous searching if conditions are more optimal. Then statistically, each myocyte spends most of the time in the more optimal direction. In skeletal muscle the proposed mechanism of cell orientation cannot work because their cells are extremely long, and may extend over the whole length of the muscle.

Interestingly, feedback through regionally sensed fiber stress is not a compelling condition for proper control of cardiac mass and structure by mechanical load. If generated left ventricular pressure is lower than required by the systemic blood pressure control system, sympathic stimuli will globally enhance contractility, causing restoration of arterial pressure. This global sympathic stimulus may also affect growth, for instance by changing intracellular calcium concentration. In the simulation the global stimulus to increase contractility above normal was used as stimulus to growth. This may simulate global cardiac mass increase due to athletic activities or pathological causes of increased hemodynamic load. Regional differences in growth are mainly controlled by feedback through early-systolic stretch. If in some region the cardiac wall is too thin, this region is stretched during the early systolic phase, causing mass to increase regionally according to Eq. 15. So, there is always a tendency to strengthen weak regions specifically by this mechanism.

The mechanical properties of the passive matrix of the myocardium are complicated as indicated by prestresses found in the cardiac wall (Omens and Fung, 1990). To our best knowledge, transmural differences in stiffness of the cardiac wall are not documented systematically. More qualitatively, when piercing the cardiac wall with a blunt needle, the outer layers feel much stiffer than the deeper layers. In these layers during ejection deformation is much larger, suggesting that the myocardial material is more compliant in regions with large deformation. In the model this mechanism is represented by passive dilation of the ventricular cavity if the change in sarcomere length during the ejection phase exceeds the normal level.

Starting from a certain initial condition, optimization resulted in a solution jiggling continuously around a stationary average (Figs. 5 and 6). Not finding a stable optimum is inherent in decentralized optimization, which can be seen as follows. Assume that the true optimum for the whole system is found. Then regional residuals remain. After decentralization of optimization, regionally a better optimum is found, causing the total solution to worsen. If in a certain region mismatch becomes large, this region will correct faster, thus limiting worsening. This process will never stop.

When changing hemodynamic load, the model behaves quite physiologically. The time scale was expressed in an arbitrary unit of an adaptation cycle, and depended on the feedback constants used. In the embryonic heart adaptation occurs probably within a few days, and in adult humans within a few weeks. In Fig. 6, mass control occurs with a time constant of 10–15 adaptation cycles. Comparing the latter value with that in the simulation, in adult humans 1–2 days is the equivalent of the duration of an adaptation cycle in the simulation.

After chronic increase of stroke volume (Fig. 6), in the first phase the volume of the left ventricular cavity increased above the stationary level reached after adaptation. Then, both cavity volume and wall volume were increased proportionally. After chronic increase of aortic pressure (Fig. 6) first left ventricular pressure was maintained by an increase of contractility. As a result total wall mass increased. Interestingly, end-diastolic left ventricular volume decreased with increasing pressure load. At a certain level of pressure load,

end-diastolic volume approached stroke volume, causing the ejection fraction to approach 100%. In the simulation the related limiting pressure was calculated to be approximately 30 kPa (225 mm Hg). Above this pressure, growth control was not possible anymore. Chronic malignant hypertension is known to result in heart failure. In the simulation an increase of systolic pressure modified fiber structure. This adaptation of the fiber angle seemed to be reversible. It is not known yet if this adaptation to pressure is realistic.

The transmural course of fiber direction as found in the simulations (Figs. 5 and 7) was not significantly different from anatomical findings (Fig. 7). The variation between different animals and conditions is quite large, especially on the endocardial side. On this side variations are probably large because in the experiments the boundary between wall and cavity is not well defined due to large indentations of the inner myocardium. Various investigators may have used different criteria for positioning of the inner boundary (Ross and Streeter, 1975). The influence of mechanical effects from the right ventricle and the papillary muscles on fiber direction is as yet unknown. Also, the effects of invalidity of the cylindrical model near base and apex are not known. These effects can only be studied adequately by means of a three-dimensional analysis of cardiac mechanics.

The kinematics of the cylindrical model was based on earlier studies (Arts et al., 1991). To our best knowledge the longitudinal shear mode enabling endocardial axial shortening at the cost of epicardial axial lengthening has not been described previously. In the model this mode is important at the long run because it balances the forces of the fibers in the inner layers with those in the outer layers. For pump function during the cardiac cycle this mode seems less important, as the related motion (k_2) seems to be small (Table 1).

We do not want to suggest that cardiac growth is stimulated exclusively by stretch, shortening, and contractility. It has been established that the injection of crude extracts from hypertrophied cardiac tissue can elicit hypertrophy in vivo without any change in the hemodynamic state (Hammond et al., 1979). Another indication for the existence of autocrine or paracrine regulating factors is that the transforming growth factor β (TGFβ) and the basic fibroblast growth factor (bFDG) are both able to provoke the expression of fetal cardiac genes when added to isolated myocytes. Both growth factors are induced after hemodynamic overload in vivo, as well as by expression of the latter set of fetal genes (Izumo et al., 1988; Parker and Schneider, 1991). This suggests that the process of cardiac hypertrophy can be elicited directly by substrates without interference of mechanical stimuli. It is not known yet, to what extent the pathway through these substrates is used by regular control of growth by mechanical load.

CONCLUSIONS

When simulating the left ventricle by a cylinder consisting of muscle fibers embedded in a compliant incompressible tissue, stresses and strains of the fibers were calculated. Assuming that in the environment of each cardiac cell (1) end-diastolic sarcomere length, (2) early systolic sarcomere stretch, (3) systolic sarcomere shortening, and (4) global contractility can be sensed, a control mechanism was designed for adaptation of cell mass, stiffness of the passive structures, and cellular orientation in the field of deformation. As a result of all individual regional control actions, a stable transmural distribution of fiber direction and a physiological adaptation of wall mass and cavity volume to hemodynamic load was obtained. The simulated transmural course of fiber direction was not significantly different from anatomical findings. During operation the solution varied continuously, but within limits. Deviations occurring in the cardiac structure were corrected intrinsically. Interestingly, regional feedback through fiber stress was not a compelling condition for proper adaptation of the cardiac shape and structure to hemodynamic load.

APPENDIX

Deformation mode radial gradient of axial strain

A mode of deformation should be found so that for $v = 0$ the enclosed volume remains constant, whereas the fibers in the outer layers can shorten, causing stretch of the fibers in the inner layers. Deformation of the incompressible cylinder is rotationally symmetric. So, for the radial, circumferential, and axial extensions e_{rr}, e_{cc}, and e_{zz} it holds:

$$e_{rr}e_{cc}e_{zz} = 1 \tag{A1}$$

Because of rotational symmetry, radial and circumferential extensions are coupled. In a cylinder the volume enclosed is proportional to r^2, the property that is used to convert radial differentials to differentials with respect to v. It holds:

$$e_{rr} = e_{cc} + r\partial e_{cc}/\partial r = e_{cc} + 2(u + v)\partial e_{cc}/\partial v \tag{A2}$$

Multiplying Eq. A2 by e_{cc}, rewriting the differential, and using Eq. A1 results in:

$$e_{rr}e_{cc} = \partial[(u + v)e_{cc}^2]/\partial v = 1/e_{zz} \tag{A3}$$

A relatively simple relationship for e_{zz} is chosen:

$$e_{zz} = \frac{1}{1 + 4k_2v/u} \tag{A4}$$

After integration of Eq. A3 with respect to v and using $e_{cc} = e_{zz} = 1$ for $k_2 = 0$ and $v = 0$, for circumferential extension e_{cc} it is found:

$$e_{cc} = [1 + 2k_2v^2/(u^2 + uv)]^{0.5} \tag{A5}$$

Eq. A5 has been applied to obtain Eq. 4.

REFERENCES

Aoyagi, T., I. Mirsky, M. F. Flanagan, J. J. Currier, S. D. Colan, and A. M. Fujii. 1992. Myocardial function in immature and mature sheep with pressure-overload hypertrophy. *Am. J. Physiol.* 262:H1036–H1048.

Arts, T., P. H. M. Bovendeerd, F. W. Prinzen, and R. S. Reneman. 1991. Relation between left ventricular cavity pressure and volume and systolic

fiber stress and strain in the wall. *Biophys. J.* 59:93–103.

Arts, T., W. C. Hunter, A. Douglas, A. M. M. Muijtjens, and R. S. Reneman. 1992. Description of the deformation of the left ventricle by a kinematic model. *J. Biomech.* 25:1119–1128.

Arts, T., and R. S. Reneman. 1989. Dynamics of left ventricular wall and mitral valve mechanics: a model study. *J. Biomech.* 22:261–271.

Arts, T., P. C. Veenstra, and R. S. Reneman. 1979. A model of the mechanics of the left ventricle. *Ann. Biomed. Eng.* 7:299–318.

Bovendeerd, P. H. M., T. Arts, J. M. Huyghe, D. H. Van Campen, and R. S. Reneman. 1992. Dependence of left ventricular wall mechanics on myocardial fiber orientation: a model study. *J. Biomech.* 25:1129–1140.

Campbell, S. E., B. Korecky, and K. Rakusan. 1991. Remodeling of myocyte dimensions in hypertrophic and atrophic rat hearts. *Circ. Res.* 68: 984–996.

Chadwick, R. S. 1982. Mechanics of the left ventricle. *Biophys. J.* 39: 279–288.

Chapman, D., K. T. Weber, and M. Eghbali. 1990. Regulation of fibrillar collagen types I and III and basement membrane type IV collagen gene expression in pressure overloaded rat myocardium. *Circ. Res.* 67: 787–794.

Contard, F. C., V. Koteliansky, F. Marotte, I. Dubus, L. Rappaport, and J. L. Samuel. 1991. Specific alterations in the distribution of extracellular matrix components within rat myocardium during development of pressure overload. *Lab. Invest.* 64:65–75.

De Tombe, P. P., and H. E. D. J. Ter Keurs. 1991. Sarcomere dynamics in cat cardiac trabeculae. *Circ. Res.* 68:588–596.

Flaherty, J. T., J. E. Pierce, V. J. Ferrans, D. J. Patel, W. Kirk, and D. L. Fry. 1972. Endothelial nuclear patterns in the canine arterial tree with particular reference to hemodynamic events. *Circ. Res.* 30:23–33.

Gaasch, W. H., C. W. Andrias, and H. J. Levine. 1978. Chronic aortic regurgitation: the effect of aortic valve replacement on left ventricular volume, mass and function. *Circulation.* 58:825–836.

Gelpi, R. J., A. Pasipoularides, A. S. Lader, T. A. Patrick, N. Chase, L. Hittinger, R. P. Shannon, S. P. Bishop, and S. F. Vatner. 1991. Changes in diastolic cardiac function in developing and stable perinephritic hypertension in conscious dogs. *Circ. Res.* 68:555–567.

Grimm, A. F., H. L. Lin, and B. R. Grimm. 1980. Left ventricular free wall and intraventricular pressure sarcomere length distributions. *Am. J. Physiol.* 239:H101–H107.

Hammond, G. L., E. Wieben, and C. L. Markert. 1979. Molecular signals for initiating protein synthesis in organ hypertrophy. *Proc. Natl. Acad. Sci. USA.* 76:2455–2459.

Hill, A. V. 1950. A discussion on muscular contraction and relaxation: their physical and chemical basis. *Proc. Roy. Soc. Lond. B.* 137:40–87.

Huyghe, J. M., D. H. Van Campen, T. Arts, and R. M. Heethaar. 1991. A two-phase finite element model of diastolic left ventricle. *J Biomech.* 24, 527:538.

Izumo, S., B. Nadal-Ginard, and V. Mahdavi. 1988. Protooncogene induction and reprogramming of cardiac gene expression produced by pressure overload. *Proc. Natl. Acad. Sci. USA.* 85:339–343.

Komuro, I., T. Kaida, Y. Shibazaki, M. Kurabayashi, Y. Katoh, E. Hoh, F. Takaku, and Y. Yazaki 1990. Stretching cardiac myocytes stimulates proto-oncogene expression. *J. Biol. Chem.* 265:3595–3598.

Mann, D. L., R. L. Kent, and G. Cooper IV. 1989. Load regulation of the properties of adult feline cardiocytes: growth induction by cellular deformation. *Circ. Res.* 64:1079–1090.

McDermott, P. J., L. I. Rothblum, S. D. Smith, and H. E. Morgan. 1989. Accelerated rates of ribosomal RNA synthesis during growth of contracting heart cells in culture. *J. Biol. Chem.* 264:18220–18227.

Monrad, E. S., O. M. Hess, T. Murakami, H. Nonogi, W. J. Coriu, and H. P. Krayenbühl. 1988. Time course of regression of left ventricular hypertrophy after aortic valve replacement. *Circulation.* 77:1345–1355.

Mukherjee, D., and S. Sen. 1990. Collagen phenotype during development and regression of myocardial hypertrophy in spontaneously hypertensive rats. *Circ. Res.* 67:1474–1480.

Omens, J. H., and Y. C. Fung. 1990. Residual strain in rat left ventricle. *Circ. Res.* 66:37–45.

Parker, T. G., and M. D. Schneider. 1991. Growth factors, proto-oncogenes, and plasticity of the cardiac phenotype. *Annu. Rev. Physiol.* 53:179–200.

Peskin, C. S. 1989. Fiber architecture of the left ventricular wall: an asymptotic analysis. *Commun. Pure Appl. Math.* 42:79–113.

Pollack, G. H., and J. W. Krueger. 1976. Sarcomere dynamics in intact cardiac muscle. *Eur. J. Cardiol.* 4(Suppl.):53–65.

Prinzen, F. W., C. H. Augustijn, T. Arts, M. A. Allessie, and R. S. Reneman. 1990. Redistribution of myocardial fiber strain and bloodflow by asynchronous activation. *Am. J. Physiol.* 259:H300–H308.

Prinzen, F. W., T. Delhaas, T. Arts, and R. S. Reneman. 1994. Asymmetrical changes in ventricular wall mass by asynchronous electrical activation of the heart. *In* Interactive Phenomena in the Cardiac System. S. Sideman and R. Beyar, editors. Plenum Publishing Corp., New York. In press.

Ross, M. A., and D. D. Streeter. 1975. Non-uniform subendocardial fiber orientation in the macaque left ventricle. *Eur. J. Cardiol.* 3:229–247.

Rubany, G. M., A. D. Freay, K. Kauser, A. Johns, and D. R. Harder. 1990. Mechanoreception by the endothelium: mediators and mechanisms of pressure- and flow-induced vascular responses. *Blood Vessels* 27: 246–257.

Sadoshima, J. I., L. Jahn, T. Takahashi, T. J. Kulik, and S. Izumo. 1992a. Molecular characterization of stretch-induced adaptation of cultured cardiac cells. *J. Biol. Chem.* 267:10551–10560.

Sadoshima, J. I., T. Takahashi, L. Jahn, and S. Izumo. 1992b. Roles of mechano-sensitive ion channels, cytoskeleton, and contractile activity in stretch-induced immediate-early gene expression and hypertrophy of cardiac myocytes. *Proc. Natl. Acad. Sci. USA.* 89:9905–9909.

Samuel, J. L., A. Barrieux, S. Dufour, I. Dubus, F. Contard, V. Koteliansky, F. Farhadian, F. Marotte, J.-P. Thiéry, and L. Rappaport. 1991. Accumulation of fetal fibronectin mRNA's during the development of rat cardiac hypertrophy induced by pressure overload. *J. Clin. Invest.* 88: 1737–1746.

Sasayama, S., J. Ross, and D. Franklin. 1976. Adaptations of the left ventricle to chronic pressure overload. *Circ. Res.* 38:172–178.

Shigematsu, S., K. Hiromatsu, T. Aizawa, T. Yamada, N. Takasu, A. Niwa, Y. Miyahara, M. Tsujino, and Z. Schimizu. 1990. Regression of left ventricular hypertrophy in patients with essential hypertension: outcome of 12 years antihypertensive treatment. *Cardiology* 77:280–286.

Sigurdson, W., A. Ruknudin, and F. Sachs. 1992. Calcium imaging of mechanically induced fluxes in tissue cultured chick heart: role of stretch-activated ion channels. *Am. J. Physiol.* 262:H1110–H1115.

Streeter, D. D. 1979. Gross morphology and fiber geometry of the heart. *In* The Cardiovascular System, the Heart. R. M. Berne, editor. American Physiological Society, Bethesda, MD. 61–112.

Ter Keurs, H. E. D. J., W. H. Rijnsburger, R. Van Heuningen, and M. J. Nagelsmit. 1980. Tension development and sarcomere length in rat cardiac trabeculae: evidence of length-dependent activation. *Circ. Res.* 46: 703–714.

Torrent-Guasp, F. 1959. An Experimental Approach on Heart Dynamics. Aguirre Torre, Madrid.

Van der Vusse, G. J., T. Arts, J. F. C. Glatz, and R. S. Reneman. 1990. Transmural differences in energy metabolism in the left ventricular myocardium: fact or fiction. *J. Moll. Cell. Cardiol.* 22:23–27.

Waldman, L. K., Y. C. Fung, and J. W. Covell. 1985. Transmural myocardial deformation in the canine left ventricle. Normal in vivo three-dimensional finite strain. *Circ. Res.* 57:152–163.

Watson, P. A. 1991. Function follows form: generation of intracellular signals by cell deformation. *FASEB J.* 5:2013–2019.

Weber, K. T., J. S. Janicki, S. G. Shroff, R. Pick, R. M. Chen, and R. I. Bashey. 1988. Collagen remodeling of the pressure overloaded, hypertrophied nonhuman primate myocardium. *Circ. Res.* 62:757–765.

Yazaki, Y., I. Komuro, T. Yamazaki, K. Tobe, K. Maemura, T. Kadowaki, and R. Nagai. 1993. Role of protein kinase system in the signal transduction of stretch-mediated protooncogene expression and hypertrophy of cardiac myocytes. *Mol. Cell. Biochem.* 119, 11:16.

Yoran, C., J. W. Covell, and J. Ross. 1973. Structural basis for the ascending limb of left ventricular function. *Circ. Res.* 32:297–303.